2. Target Stratigraphy ❖❖❖

The impact event excavated material from the Colorado Plateau, which is a broad region in the Four Corners area that is composed of relatively flat lying sedimentary rocks. A flat-lying, multi-layered sedimentary target has made Barringer Meteorite Crater a particular important impact site, because the structural deformation created by the impact is relatively easy to observe.

Plateau sediments in the vicinity of the crater are ~1070 m (~3510 ft) thick and overlie a crystalline basement of continental crust (Fig. 2.1). The Devonian Martin Formation uncomformably overlies the basement, which is, in turn, unconformably covered by the Mississippian Redwall Formation. These units are covered by a Permian section that is poorly sampled in the immediate vicinity of the crater. A small amount of the Molas Formation may occur at the base of the Permian section, followed by the Naco Formation. The thickness of the latter is not well-known and is inferred on the basis of a seismic refraction horizon (Ackerman *et al.*, 1975) believed to occur between the Naco and the overlying Supai Formation (Roddy, 1978). The Supai is the thickest sedimentary unit in the section. It is covered by the Coconino Formation, Toroweap Formation, Kaibab Formation, and Moenkopi Formation, all of which are exposed in the crater walls. These units represent the upper portion of the well-known Grand Canyon sequence and are the critical units involved in the impact event (Fig. 2.1). Detailed descriptions of these latter units follow.

Coconino Sandstone. The Coconino sandstone is white, fine-grained, and saccharoidal (*i.e.*, a granular texture similar to loaf sugar) quartzose sandstone that occurs in massive beds with cross-stratification. The unit was defined in the plateau province by Darton (1910) and subsequently described in greater detail by Noble (1914) in the Grand Canyon, where outcrops of the sandstone are particularly spectacular. Sets of cross-stratified units are sometimes 30 m (100 ft) thick. The sedimentary environment was controversial for several decades, but an aeolian environment was the eventual consensus (McKee, 1934, and Reiche, 1938; *cf.*, Schuchert, 1918, and Read, 1950). Thus, the Coconino's high-angle cross-bedded laminae are fossilized sand dune slopes produced when northern Arizona was covered by a huge sand dune field similar to the modern Sahara. The Coconino thickens to the south, where it has a maximum thickness of 330 m (1000 ft ; Kieffer, 1974). In the vicinity of the impact, the Coconino is 210 to 240 m (700 to 800 ft) thick (Shoemaker, 1974). It is the basal unit excavated by the impact event. Only the upper portions of the Coconino Formation, however, are exposed in the crater walls.

The sandstone is >95% quartz. Grains are well-rounded and have dimensions that are 0.1 to nearly 4 mm, with an average length of 0.1 to 0.2 mm (Table 2.1). The sandstone is porous, but the porosity is heterogeneously distributed. Samples may have <10% porosity, but can also have 25% porosity, a variation that can influence the propagation of a shock wave and shock-metamorphic effects.

Chemical analyses of Coconino sandstone exposed in the crater walls reflect the high concentration of quartz (See *et al*., 2002). Silica (SiO_2) totals range from 96.99 to 97.54%, with an average value of 97.03 wt% (Table 2.2). The dominant impurity is Al_2O_3.

Because the Coconino sandstone is such an important target component (representing ~70% of the stratigraphic depth of the excavation cavity; calculated from reconstruction by Roddy 1978), its physical properties have been investigated experimentally (Table 2.1). Microscopic radial fracturing of Coconino occurs at tensile stresses of 30 MPa, which is a factor of 10 less than that of crystalline rocks (Ai and Ahrens, 2004) and approximately a factor of 10 higher than that measured in Kaibab samples that were recovered from the uplifted rim of the crater (Watkins and Walters, 1966).

Toroweap Formation. The Toroweap is a thin (10 ft or 3 m) layer of sandstone and dolomite at the crater. Elsewhere in northern Arizona the unit can be thicker and composed of limestone with substantial amounts of yellow sandstone and reddish mudstone. The Toroweap formed on the floor of a shallow sea that migrated into the area from the west. The sandy portions represent a fluctuating ancient shoreline of western North America during the Permian.

Much more is known about the Toroweap (*e.g.*, McKee, 1938) than will be summarized here, because the formation is such a thin unit at the crater. In other areas of northern Arizona, the limited stratigraphic extent of the Toroweap is partly the result of erosion, because the contact between the Toroweap and overlying Kaibab is normally unconformable (McKee, 1938). At the crater, however, the limited stratigraphic thickness appears to reflect limited sedimentation, because Shoemaker (1974) describes the contact between the Toroweap and Kaibab as conformable.

The Toroweap is not quite as pure a quartz sandstone as the Coconino (Table 2.2). It contains additional Al_2O_3 and probably carbonate (reflected by enhanced Mg, Ca, and LOI abundances). The average silica abundance is 93.34 wt%.

Kaibab Formation. The Kaibab Formation at the crater is 260 to 265 ft (79 to 81 m) thick and composed of dolomite, dolomitic limestone, and thin calcareous sandstone horizons. Fossil shells are apparent (Fig. 2.2), although preservation is often poor because of diagenesis. One also finds preserved burrows of marine organisms that lived and fed in the sea-floor sediments. The Kaibab was deposited in a low-energy marine environment during the Permian over 250 million years ago.

The first report of a thick magnesian limestone (dolomite) was provided by Jules Marcou in a report from the 1853-54 expedition across northern Arizona that was led by Lieutenant Whipple (and, hence, popularly known as the Whipple Survey). Once called the Aubrey limestone, the unit was renamed the Kaibab limestone in 1910 when the USGS assigned the term Aubrey to a larger group of rocks that contained the magnesian limestone. A formal description of the Kaibab Formation was produced by McKee (1938), who measured sections throughout the region, including several sections in the vicinity of Meteor Crater. These sections occur in Walnut Canyon, in Padre Canyon at Hwy 66, at an outcrop ~10 miles southwest of Winslow, and at several locations along Clear Creek. McKee (1938, p. 8) briefly describes 150 ft of Kaibab at Meteor Crater, although Shoemaker (1960) measured 260 to 265 ft (79 to 81 m). In general, the Kaibab thins regionally from the north to south or northwest to southeast.

The Kaibab has three members that are designated alpha (α), beta (β), and gamma (γ) from the top to the bottom of the sequence (Fig. 2.1). The oldest member (γ) represents a time of advancing seas, the middle member (β) the time with the most extensive seas, and the youngest member (α) a time of receding seas. Sand units mixed with the uppermost (α) dolomite beds have been interpreted as a shoreline facies. They also erode in different fashions, as illustrated in the crater walls. The α and γ members form cliffs, whereas the β member often erodes to form a slope. In outcrop, one finds that diagenesis and weathering have conspired to produce a distinctive vuggy texture (Fig. 2.2) that is commonly called tear-pants for obvious reasons.

The Kaibab varies horizontally (geographically), which McKee (1938) divided into several facies. Facies 3 of the α member, facies 4 of the β member, and facies 3 of the γ member of the Kaibab occur at Barringer Crater (Fig. 2.3). Facies 3 of the α member contains trilobites (*Ditomopyge*), brachiopods (*Chonetes*, *Marginifera*, and *Productus bassi*), cephalopods (*Orthoceras* and *Plagioglypta*), gastropods (*Pleurotomaria*, *Euphemus*, *Bellerophon*, *Euomphalus*, *Bucanopsis*, and *Naticopsis*), and pelecypods (*Allorisma*, *Leda*, *Astartella*, *Pleurophorus*, *Nucula*, and *Schizodus*). Facies 4 of the β member contains brachiopods (*Pugnoides* and *Hustedia*), pelecypods (*Schizodus*, *Leda*, *Pleurophorus*, *Deltopecten*, and *Myalina*), and a long-stem echinoid (*Archaeocidaris*).

Because the Kaibab Formation is an important target unit at the crater, a NASA-sponsored drilling project recovered several cores from the rim of the crater and one core from a distant site unaffected by the impact event (Watkins, 1966). The latter was analyzed to provide pre-impact properties of the Kaibab (Watkins and Walters, 1966), which are summarized in Table 2.3 (drill core hold KC-2). These samples were recovered from Kaibab that was buried by a basalt lava flow associated with the SP cinder cone north of Flagstaff. This hole penetrated the same Kaibab α and β facies as those exposed at the impact site (Fig. 2.3). Measurements of recovered sample include porosity, permeability, compressive strength, tensile strength, Poisson's ratio, Young's modulus, the shear modulus, bulk modulus, and compressional and shear velocities.

Five boreholes were drilled along the southern crater rim. Two of the holes (MCC-3 and MCC-4) provide most of the data. The MCC-3 hole is located about 150 m south of the modern topograpihc rim of the crater. Drill core hole MCC-4 is located 10 m south of the modern topographic rim of the crater. These holes penetrated impact ejecta, Moenkopi, and Kaibab, although physical measurements were not always tied to these lithologies. Physical properties from a depth of 21 to 31 m (69 to 102 ft) in MCC-3 are listed in Table 2.4. Abrupt changes in Young's, shear, and bulk modulii suggest a lithologic change at a depth of ~29 m. Samples in the 29 to 31 m interval may be tied to Kaibab, because those values in the MCC-3 data (Table 2.4) are similar to those of Kaibab in the KC-2 data (Table 2.3).

Lithological control in borehole MCC-4 is better than that in MCC-3, as shown in Tables 2.5 and 2.6. In this hole, the Kaibab begins at a depth of 21 m and continues to the bottom of the hole at 106 m. The thickness of the Kaibab in the core (~85 m) is similar to that measured in outcrop (79 to 81 m). The porosity in core samples ranges from ~2% (in dolomite) to ~30% (in some sandstone horizons). The permeability is equally variable.

Because Kaibab is composed of both dolomite and sandstone, carbonate fractions range from 20 to 97 vol% with quartz being responsible for most of the remaining material (Table 2.6; Haines, 1966). The carbonate fractions generally increase with stratigraphic height. Petrographically, dolomite occurs as (i) a microcrystalline matrix with smaller fraction of subangular to subrounded quartz grains, the latter of which are well sorted with an average diameter of 0.1 mm; (ii) microcrystalline clasts, in which grain diameters are ~0.01 mm and clast diameters range from 0.5 to 7 mm, with an average of 2.5 mm diameter; (iii) as anastomosing stringers, and (iv) coarse anhedral grains with diameters of 0.5 to 4 mm (Haines, 1966). The unit also contains minor plagioclase, microcline, and opaque minerals. Sericite occurs at one specific stratigraphic interval.

The composition of the Kaibab varies with stratigraphic position as the beds vary between different mixtures of sand and dolomite. Silica in 12 stratigraphic subdivisions of the Kaibab ranges from 16.36 to 57.43 wt%, with an average of 38.32 wt% (Table 2.2; See *et al.*, 2002). Dolomite (MgO, CaO, and CO_2) dominate the remainder of the material in the samples, but ~2 wt% Al_2O_3 and Fe_2O_3 also occur in the unit.

Moenkopi Formation. The strikingly red Moenkopi is the lower of two Triassic sedimentary sequences that dominate the Painted Desert province. Interestingly, the Moenkopi and the underlying yellowish Kaibab span the Permian-Triassic boundary, which represents the largest mass extinction event in the marine record during the Phanerozoic. The contact between these two formations is unconformable, however, so sediments deposited precisely at the P-T boundary do not exist and the sequence cannot be used to determine the cause of the P-T mass extinction event. One hypothesis being explored elsewhere in the world is that the P-T mass extinction, like the Cretaceous-Tertiary (K-T) event that claimed dinosaurs and 75% of the species on Earth, was caused by an impact event far larger in scale than that represented by Barringer Crater.

In the vicinity of the crater, the Moenkopi Formation is comoposed of two members: Wupatki and Moqui (McKee, 1954). An uppermost Holbrook Member and the overlying Chinle Formation do not occur in the vicinity of the crater, although the latter is abundant to the east, northeast, and north. Where covered by the Chinle (and, thus, not eroded), the Moenkopi can reach a thickness of 600 to 700 feet (183 to 213 m). In the walls of the crater, however, the Moenkopi ranges from only 7 to 30 ft (2 to 10 m).

Some of the beds of Moenkopi are a calcareous siltstone with an iron-rich matrix. Within the MCC-4 core, quartz content of the siltstone varied from 55 to 80%, the remainder being composed of carbonate (Table 2.6). Porosity ranged from 7.5 to 18.2% and the permeability is low. Quartz is subrounded, equant, and well-sorted, with an average diameter of 0.1 mm (Haines, 1966). Some of the quartz recovered in the MCC-4 core has wavy extinction. Calcite is typically coarser (0.2 mm average) than the quartz. It also envelopes quartz and has anhedral margins, indicating a secondary origin. Diagenetic growth of calcite nodules, up to 6 mm, with embedded quartz occurs in some intervals (Haines, 1966). Other detrital grains include feldspar and unidentified opaque material in trace amounts. The matrix is very fine-grained and not well-characterized, but is stained by iron. The Moenkopi also contains fissile intervals that contain abundant sericite and muscovite (Haines, 1966).

Those mineral assemblages produce strata with compositions that are moderately silicious (averaging 65.30 wt% SiO_2) and also contain significant quantities of CaO (and presumably CO_2), Al_2O_3, Fe_2O_3, FeO, and K_2O (Table 2.2).

Moenkopi sediments were deposited on a coastal floodplain at the edge of a sea, similar to modern Louisiana. Many of the beds were deposited on intertidal mud flats, where several sedimentary features were produced (Fig. 2.4): dessication (mud) cracks, longitudinal and interference ripple marks (the latter indicating conflicting current directions), sole marks, worm and shrimp burrows that wander across slabs, raindrop impressions, reptile and amphibian trackways, and abundant fossils. One of the most important fossil quarries in the Moenkopi is located at the crater (Camp et al., 1947; Peabody, 1948; Welles and Cosgriff, 1965).

A University of California excavation team worked the site in the 1930's. The finds include tetrapod tracks with beaded skin surfaces and over 20 skulls. Track ways produced by multiple species of amphibians and reptiles were recovered (Fig. 2.5). Some of the skulls represented a new species of capitosaurid amphibian (Fig. 2.6). The type specimen from the quarry is called *Parotosaurus peabodyi* (Welles and Cosgriff, 1965).

The basal Wupatki Member begins with a red, thin (~1 ft thick) fissile shale, although this shale does not outcrop in all locations around the crater. The Wupatki Member is dominated by a cross-bedded, but relatively massive unit that outcrops as a rounded pink ledge-forming unit that often erodes into a series of orbicular knobs. The unit is 2 to 6 m (7 to 20 ft) thick. Outcrops of the Wupatki Member form a veneer on the landscape in the immediate vicinity of the crater.

Stratigraphically above the Wupatki Member is a dark red siltstone and sandstone unit about 8 m (25 ft) thick that is called the Moqui Member of the Moenkopi (Shoemaker and Kieffer, 1974). This unit is very fissile compared to the Wupatki member. The overturned sequence usually occurs in this unit, which, because of its fissile nature, makes it difficult to put one’s finger on the contact between upright and overturned Moenkopi in the rim sequence. (See discussion in Chapter 6).

The Moenkopi is a well-known building stone at the crater and elsewhere in the region. The first museum at the crater (on northwest crater rim) and another building (on southwest ejecta blanket) were built of the stone, as was Harvey Nininger’s American Meteorite Museum that existed along Highway or Route 66 from 1946 through 1953. In Flagstaff, the Babbitt Brothers Building (built between 1888 and

1891), Atlantic and Pacific Railroad Depot (1889), Old Main at Northern Arizona University (1894), and the Coconino County Courthouse (1894-95) are built with blocks of Moenkopi, which is often called Arizona Red Sandstone.

Pre-impact Structure

The impact occurred in a relatively flat lying sequence of these Permian and Triassic sediments. Folds in the region are evident, but subtle. Synclines and anticlines occur within a few kilometers of the crater and the impact occurred on a gentle monoclinal fold (Fig. 2.7; Shoemaker, 1960). Although a thin-veneer of Moenkopi occurs at the crater, it is absent around Canyon Diablo and over a vast region to the west of the crater. The presence of Moenkopi at the impact site is fortuitous, however, because it greatly assists in interpretation of crater formation (as discussed in Chapter 6). Target sediments are also cross-cut by NW-SE trending normal faults (Fig. 2.7) that may be many kilometers long, but only have offsets of a few to about 30 m (Shoemaker, 1987). The region is also cross-cut by a strong set of joints that can extend for hundreds of meters (Kelley and Clinton, 1960), with pre-impact orientations of that seem to have formed a conjugate NW-SE and weaker SW-NE. Roddy (1978) measured the joints within a few kilometers of the crater and found the most prominent orientations in Moenkopi are 293° (with a range of 290 to 297°) and in Kaibab are 304° (with a range of 301 to 308°). A secondary set is oriented 23° (with a range of 10 to 32°) in the Moenkopi and 30° (with a range of 17 to 36°) in the Kaibab. As Roddy (1978) describes, these joints remain vertical in canyon walls down to depths of 100 m in the region and have been implicated in the unusually square shape of the impact crater (Shoemaker, 1960, 1987), as discussed further in the next chapter.

Topography at the time of impact

Pre-impact topography can be inferred from the existing topography, because the crater is so young and erosion may have been small. (See Chapter 7 for discussion of post-impact erosion.) A better measure of the topography at the time of impact, however, can be made using the topography visible in the crater walls and buried beneath impact ejecta. As discussed above, the Moenkopi in the crater walls varies in thickness from 2 to 10 m, implying topography up to 8 m. A drilling campaign through the ejecta blanket revealed buried topography with an average relief of 5 to 10 m and a maximum of 23 m (Roddy *et al.*, 1975). Grant and Schultz (1993) used ground-penetrating radar to image the subsurface on the west side of the crater. They found Moenkopi ridges beneath the ejecta blanket that were approximately 200 m wide and 5 m high. Gilbert (1896) also tried to reconstruct the topography before the crater formed. He extended existing topographic contours beyond the crater ejecta blanket towards crater center. His method assumes there has been little erosion since the crater formed. His restored topographic map suggests variation of about 3 m and the possibility of a small SW-NE stream channel at the point of impact.

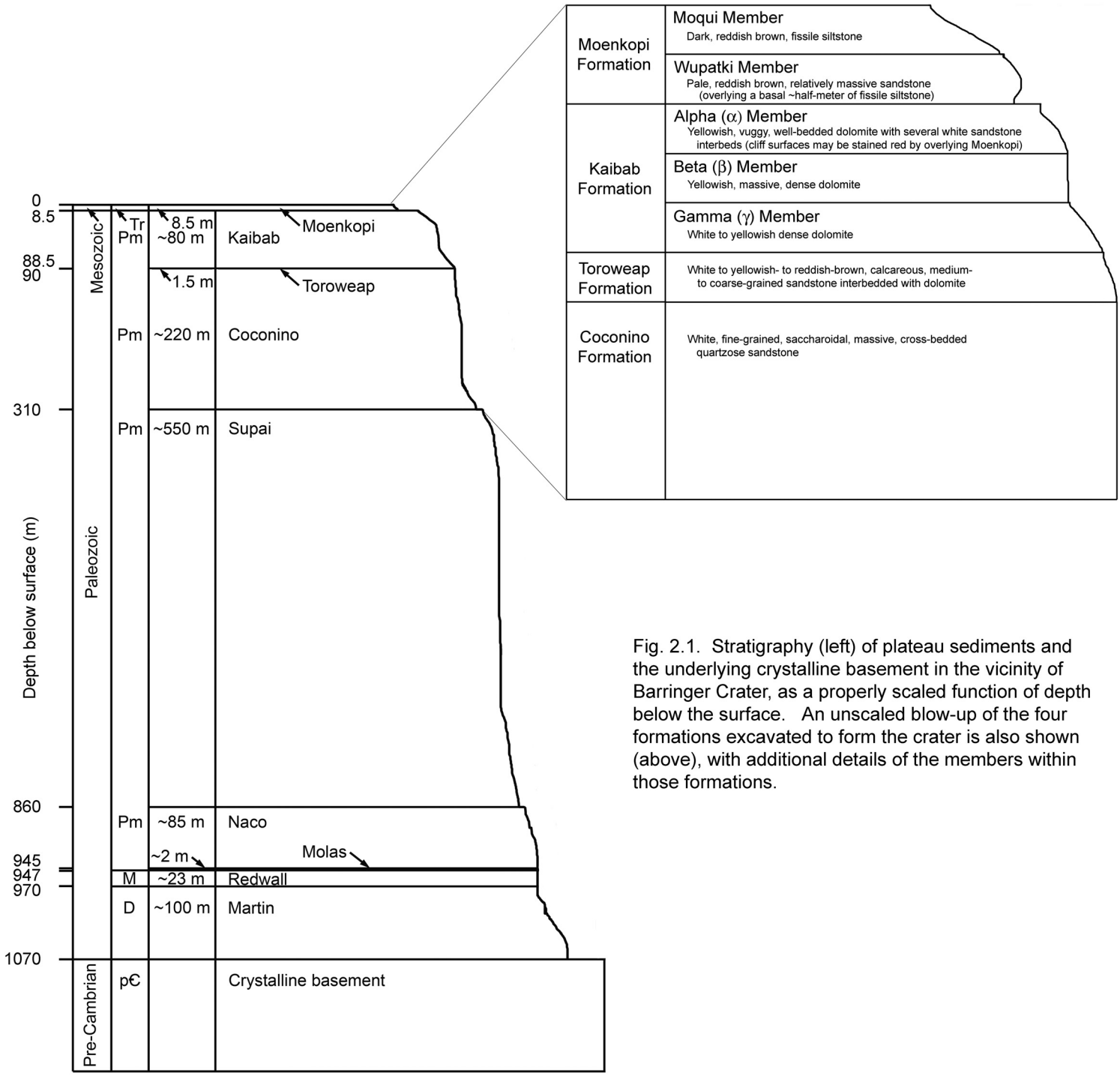

Fig. 2.1. Stratigraphy (left) of plateau sediments and the underlying crystalline basement in the vicinity of Barringer Crater, as a properly scaled function of depth below the surface. An unscaled blow-up of the four formations excavated to form the crater is also shown (above), with additional details of the members within those formations.

Table 2.1. Physical properties of the Coconino Formation

Bulk density (g/cm^3)	Grain density (g/cm^3)	Quartz (vol%)	Feldspar (vol%)	Other minerals	Average grain size (mm)	Modal grain size (mm)	Porosity (%)	Crushing strength dry ($dynes/cm^2$) (10^8)	Crushing strength H_2O sat. ($dynes/cm^2$) (10^8)	Tensile strength (MPa)	Cp (km/s)	Cs (km/s)	Reference
1.99	-	97	3	-	0.12-0.15	-	24-25	-	-	-	-	-	1
1.98	2.67	97	3	tr	0.117	0.149	25	3.14	3.64	-	-	-	2
-	-	>95	<1	<4	0.19	-	9-18*	-	-	-	-	-	3
-	-	>95	<1	<4	0.19	-	<10**	-	-	-	-	-	3
2.08	-	-	-	-	-	-	-	-	-	17***	2.81	1.82	4
2.08	-	-	-	-	-	-	-	-	-	20****	2.81	1.82	4

* for massive Coconino sandstone beds
** for laminated Coconino sandstone beds
*** for strain rate of $1/2.4 \times 10^6$/s
**** for strain rate of $1/1.4 \times 10^6$/s
Data tabulated as published. To compare the crushing and tensile strengths, 3.14 and 3.64×10^8 $dynes/cm^2$ = 31.4 and 36.4 MPa

References: (1) Ahrens and Gregson, 1964; (2) Shipman *et al.* , 1971; (3) Kieffer, 1971; (4) Ai and Ahrens, 2004

Table 2.2. Compositions of target lithologies at Barringer Meteorite Crater*

Formation	Stratigraphic thickness (m)	Cumulative target rock thickness (m)	SiO_2	TiO_2	Al_2O_3	Fe_2O_3	FeO	MnO	MgO	CaO	Na_2O	K_2O	P_2O_5	LOI	Total
Moenkopi	12.3	12.3	65.30	0.43	7.67	2.63	1.88	0.06	0.99	10.17	0.02	1.42	0.11	11.05	99.10
Kaibab	73	85.3	38.32	0.12	2.02	2.05	0.16	0.03	11.57	19.31	0.03	0.51	0.19	27.29	99.57
Toroweap	1.4	86.7	93.34	0.08	2.02	0.73	0.17	0.01	0.88	1.07	0.00	0.38	0.06	2.14	100.16
Coconino	34.4	121.1	97.03	0.07	1.49	0.67	0.05	0.00	0.06	0.12	0.00	0.19	0.03	0.51	99.55

* See *et al.* (2002); analyses of individual stratigraphic intervals can also be found in that source.

Fig. 2.2. Fossils (a-c) and diagenetic features (d) in the Kaibab Formation. Fossils are apparent in the unit, but are often poorly preserved because of diagenetic alteration (a). Better examples can be found, albeit rarely, as illustrated by the two specimens (b-c) recovered by Meteor Crater Enterprises staff. Tear-pants weathering of Kaibab surfaces (d) reflects the mix of carbonate, sulphate, and silica fluids involved in the formation of the dolomite. In the alpha member of the Kaibab, a prominent diagenetically-altered bed is often described as the yellow vuggy unit or yellow vuggy dolomite. It is a useful marker bed.

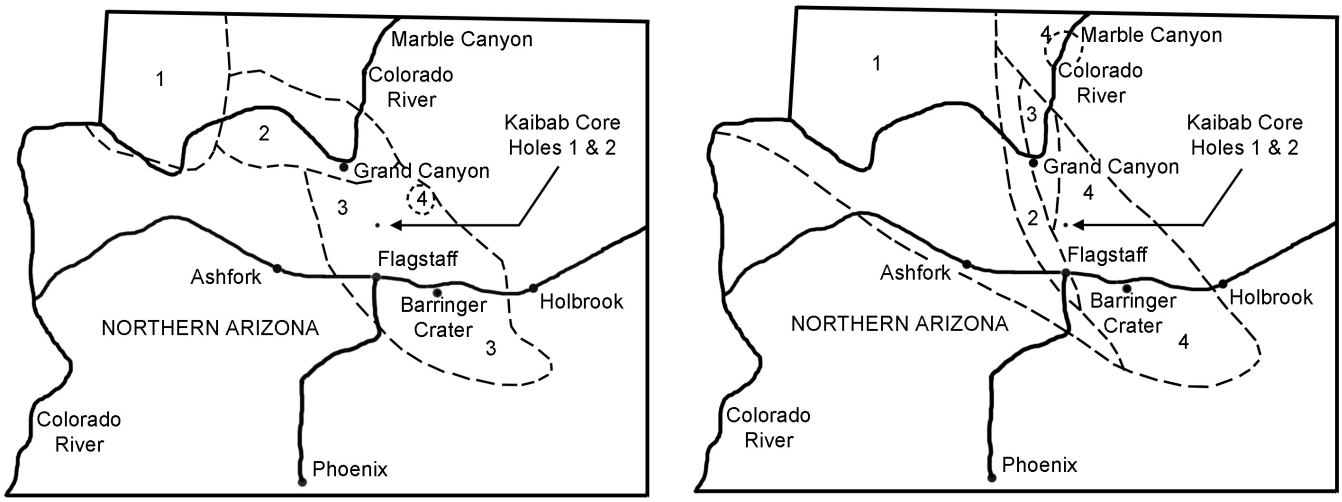

Fig. 2.3. The geographic distribution of facies within the Kaibab Formation of northern Arizona. Barringer Meteorite Crater occurs in Facies 3 of the Alpha Member (left panel) and Facies 4 of the Beta Member (right panel) of the Kaibab Formation. Drill core samples of Kaibab dolomite unaffected by the impact event were recovered in the vicinity of SP cinder cone, northwest of the crater. The Kaibab at that location represents the same facies as that at the impact crater. (Map modified from McKee, 1938.)

Table 2.3. Physical properties of the Kaibab Formation recovered from a site unaffected by impact event*

Drill core hole KC-2 (to represent unshocked Kaibab)
Located ~1 km west of the SP Crater Lava Flow

Depth (m)	Dry Bulk Density (g/cm^3)	Grain Density (g/cm^3)	Porosity (%)	Permeability (millidarcies)	Unconfined Compressive Strength ($dynes/cm^2$) (10^8)	Tensile Strength ($dynes/cm^2$) (10^7)	Poisson's Ratio	Young's Modulus ($dynes/cm^2$) (10^{11})	Shear Modulus ($dynes/cm^2$) (10^{11})	Bulk Modulus ($dynes/cm^2$) (10^{11})	V_p (mps)	V_s (mps)
						Static Measurements						
2.5	2.49	2.88	13.5	-	-	6.21	0.316	7.16	2.83	6.28	-	-
5	2.18	2.87	24	-	8.54	-	0.264	4.45	1.76	3.14	-	-
7.2	2.29	2.66	13.9	-	-	1.57	0.192	1.65	0.70	1.00	-	-
8.3	2.08	2.85	27	-	6.6	-	0.249	4.12	1.65	2.74	-	-
11.2	2.49	2.85	12.6	-	9.89	-	0.326	6.33	2.39	6.07	-	-
15.2	2.18	2.72	19.9	-	-	3.03	0.125	2.42	1.08	1.08	-	-
17.9	2.23	2.85	21.8	-	4.08	-	0.157	3.32	1.44	1.62	-	-
18.7	2.16	2.69	19.7	-	-	1.2	0.088	1.28	0.59	0.87	-	-
22.3	2.09	2.78	24.8	-	8.54	-	0.155	2.60	1.12	1.25	-	-
Avg	2.24	2.79	19.69	-	7.53	3.00	0.21	3.70	1.51	2.67	-	-
Std Dev	0.15	0.08	5.30	-	2.26	2.28	0.08	2.02	0.75	2.14	-	-
#	9	9	9	-	5	4	9	9	9	9	-	-
							Pulse Measurements					
2.5	2.49	2.88	13.5	-	-	-	0.254	7.03	2.80	4.77	5800	3400
5	2.18	2.87	24	-	-	-	0.198	4.42	1.85	2.44	4800	2900
7.2	2.29	2.66	13.9	-	-	-	0.131	1.61	0.71	0.72	2700	1700
8.3	2.08	2.85	27	-	-	-	0.205	3.82	1.58	2.16	4500	2800
11.2	2.49	2.85	12.6	-	-	-	0.237	6.63	2.68	4.20	5600	3300
15.2	2.18	2.72	19.9	-	-	-	0.147	2.85	1.24	1.34	3700	2400
17.9	2.23	2.85	21.8	-	-	-	0.245	2.91	1.16	1.90	3900	2300
18.7	2.16	2.69	19.7	-	-	-	0.06	1.45	0.69	0.55	2600	1800
22.3	2.09	2.78	24.8	-	-	-	0.209	2.78	1.15	1.60	3900	2300
Avg	2.24	2.79	19.69	-	-	-	0.187	3.72	1.54	2.19	4167	2544
Std Dev	0.15	0.08	5.30	-	-	-	0.063	1.99	0.77	1.45	1129	602
#	9	9	9	-	-	-	9	9	9	9	9	9
Avg	2.24	2.79	19.69	-	7.53	3.00	0.198	3.71	1.52	2.43	4167	2544
Std Dev	0.15	0.08	5.30	-	2.26	2.28	0.073	1.95	0.74	1.79	1129	602
#	9	9	9	-	5	4	18	18	18	18	9	9

* Watkins and Walters (1966); Core type NX, which produces a 75 mm diameter hole and a 54.8 mm diameter core
Data is tabulated as originally published. However, to convert to modern units: 1 $dyne/cm^2$ = 0.1 pascals;
thus, a tensile strength of 3.00×10^7 $dyne/cm^2$ = 3.00×10^6 pascals = 3.00 M Pa

Table 2.4. Physical properties of crater lithologies

Drill core hole MCC-3*
South side of crater, 150 meters from topographical crater rim

Depth (m)	Dry Bulk Density (g/cm^3)	Grain Density (g/cm^3)	Porosity (%)	Permeability (millidarcies)	Unconfined Compressive Strength ($dynes/cm^2$) (10^8)	Tensile Strength ($dynes/cm^2$) (10^7)	Poisson's Ratio	Young's Modulus ($dynes/cm^2$) (10^{11})	Shear Modulus ($dynes/cm^2$) (10^{11})	Bulk Modulus ($dynes/cm^2$) (10^{11})	Vp (mps)	Vs (mps)
						Static Measurements						
21.1	1.98	2.70	26.8	-	Sample too soft for testing		-	-	-	-	-	-
23.4	2.30	2.69	14.5	-	6.37	-	0.118	0.98	0.43	0.44	-	-
24.1	2.28	2.71	15.8	-	5.55	-	0.195	0.48	0.26	0.20	-	-
28.1	2.22	2.65	16.3	-	-	0.47	0.165	0.60	0.30	0.33	-	-
29.0	2.49	2.81	12.1	-	Sample too small for testing			-	-	-	-	-
29.8	2.30	2.81	18.1	-	8.68	-	0.172	3.83	1.95	1.63	-	-
30.0	2.14	2.90	26.3	-	-	2.16	0.220	1.88	1.12	0.77	-	-
30.3	2.41	2.82	14.6	-	6.44	-	0.197	4.55	2.50	1.90	-	-
30.4	2.44	2.80	12.9	-	-	2.94	0.135	6.23	2.84	2.74	-	-
Avg	2.28	2.77	17.5		6.76	1.86	0.172	2.65	1.34	1.14	-	-
Std Dev	0.16	0.08	5.4		1.34	1.26	0.036	2.24	1.09	0.96	-	-
#	9	9	9		4	3	7	7	7	7	-	-
							Pulse Measurements					
21.1	1.98	2.70	26.8	-	-	-	0.239	0.37	0.14	0.23	1470	860
23.4	2.30	2.69	14.5	-	-	-	0.235	1.01	0.41	0.64	2260	1330
24.1	2.28	2.71	15.8	-	-	-	0.194	1.98	0.83	1.07	2180	1340
28.1	2.22	2.65	16.3	-	-	-	0.052	1.28	0.61	0.47	2410	1660
29.0	2.49	2.81	12.1	-	-	-	-	-	-	-	3850	-
29.8	2.30	2.81	18.1	-	-	-	0.179	3.75	1.59	2.98	4210	2630
30.0	2.14	2.90	26.3	-	-	-	0.304	3.06	1.17	2.59	4940	2620
30.3	2.41	2.82	14.6	-	-	-	0.222	0.71	0.29	0.43	1840	1100
30.4	2.44	2.80	12.9	-	-	-	0.143	5.23	2.28	2.45	4750	3060
Avg	2.28	2.77	17.5				0.196	2.17	0.92	1.36	3101	1825
Std Dev	0.16	0.08	5.4				0.075	1.70	0.73	1.13	1331	825
#	9	9	9		4	3	8	8	8	8	9	9
Avg	2.28	2.77	17.5	-	6.8	1.86	0.185	2.40	1.11	1.26	3101	1825
Std Dev	0.16	0.08	5.4	-	1.3	1.26	0.059	1.91	0.91	1.02	1331	825
#	9	9	9		4	3	15	15	15	15	9	9

* Watkins and Walters (1966); Core type NX, which produces a 75 mm diameter hole and a 54.8 mm diameter core
Data is tabulated as originally published. However, to convert to modern units: 1 $dyne/cm^2$ = 0.1 pascals;
thus, a tensile strength of 1.86×10^7 $dyne/cm^2$ = 1.86×10^6 pascals = 1.86 M Pa

Table 2.5. Physical properties of crater lithologies and a lithologic assessment

Drill core hole MCC-4*
South side of crater, 10 meters from topographical crater rim

Depth (m)	Sub-surface elevation (m)	Dry Bulk Density (g/cm^3)	Grain Density (g/cm^3)	Porosity (%)	Permeability (millidarcies)	Lithologic Assessment**
8.2	1731.8	2.18	2.85	23.5	17.3	Ejecta - Sandstone
9.3	1730.7	2.17	2.93	25.9	2.5	Ejecta - Sandstone
10.7	1729.3	2.19	3.63	18.2	1.3	Moenkopi - Sandstone
16.0	1724.0	2.44	2.89	15.6	<0.4	Moenkopi - Sandstone
20.0	1720.0	2.48	2.68	7.5	<0.4	Moenkopi - Shaly Sandstone
21.0	1719.0	2.68	2.73	1.8	<0.4	Kaibab - Dolomite
21.4	1718.6	2.63	2.74	4.0	<0.4	Kaibab - Calc-dolomite
22.0	1718.0	2.61	2.68	2.6	<0.4	Kaibab - Dolomite
29.5	1710.5	2.44	3.04	20.0	<0.4	Kaibab - Dolomite
34.0	1706.0	2.18	2.81	23.2	26.8	Kaibab - Dolomite
37.5	1702.5	2.22	3.03	26.7	4.7	Kaibab - Dolomite
47.6	1692.4	2.39	2.99	20.1	3.8	Kaibab - Sandstone and Dolomite
54.4	1685.6	2.15	3.05	29.5	25.1	Kaibab - Sandstone and Dolomite
61.0	1679.0	2.33	2.74	15.0	1.5	Kaibab - Sandstone and Dolomite
68.0	1672.0	2.17	2.89	24.9	16.8	Kaibab - Sandstone and Dolomite
75.8	1664.2	2.14	2.72	21.3	16.7	Kaibab - Sandstone and Dolomite
81.7	1658.3	2.12	2.82	24.8	30.6	Kaibab - Sandstone and Dolomite
87.5	1652.5	2.15	3.02	28.8	37.6	Kaibab - Sandstone and Dolomite
91.5	1648.5	2.24	2.68	16.7	4.2	Kaibab - Sandstone and Dolomite
94.8	1645.2	2.35	2.91	19.2	1.7	Kaibab - Dolomite
98.3	1641.7	2.13	2.87	25.8	33.3	Kaibab - Sandstone
101.9	1638.1	2.12	2.65	22.0	80.7	Kaibab - Sandstone
105.9	1634.1	2.18	2.65	18.3	15.5	Kaibab - Sandstone
Avg		2.29	2.87	18.9	~13.9	
Std Dev		0.18	0.21	8.1	~19.1	

* Watkins and Walters (1966); core type NX, which produces a 75 mm diameter hole and a 54.8 mm diameter core
** Haines (1966); the elevation data for these lithologies are also calculated from a 1,740 m collar height provided by this author

Table 2.6. Physical and mineralogical properties of the Moenkopi and Kaibab formations.

Moenkopi Properties

Drill core hole MCC-4*,**
South side of crater, 10 meters from topographical crater rim

Depth (m)	Sub-surface elevation (m)	Carbonate (vol%)	Quartz (vol%)	Cavities (vol%)	Insoluble residue (mostly qtz) (wt%)	Dry Bulk Density (g/cm^3)	Grain Density (g/cm^3)	Porosity (%)	Permeability (millidarcies)
10.7	1729.3	-	-	-	-	2.19	3.63	18.2	1.3
11.4	1728.6	25	75	-	71.7	-	-	-	-
16.0	1724.0	-	-	-	-	2.44	2.89	15.6	<0.4
16.1	1723.9	45	55	-	-	-	-	-	-
20.0	1720.0	-	-	-	-	2.48	2.68	7.5	<0.4
20.1	1719.9	20	80	-	-	-	-	-	-

* Haines (1966); vol% determined visually in thin-section; wt% insoluble residue after acid dissolution of carbonate
** Watkins and Walters (1966)

Kaibab Properties

Drill core hole MCC-4*,**,***
South side of crater, 10 meters from topographical crater rim

Depth (m)	Sub-surface elevation (m)	Carbonate (vol%)	Quartz (vol%)	Cavities (vol%)	Insoluble residue (mostly qtz) (wt%)	Dry Bulk Density (g/cm^3)	Grain Density (g/cm^3)	Porosity (%)	Permeability (millidarcies)
21.0	1719.0	97	3	Tr	-	2.68	2.73	1.8	<0.4
21.4	1718.6	95	2	3	-	2.63	2.74	4.0	<0.4
22.0	1718.0	95	5	-	-	2.61	2.68	2.6	<0.4
22.6	1717.4	-	-	-	24.6	-	-	-	-
22.7	1717.3	65	35	-	-	-	-	-	-
23.3	1716.7	40	60	-	-	-	-	-	-
29.5	1710.5	-	-	-	-	2.44	3.04	20.0	<0.4
29.9	1710.1	75	10	15	-	-	-	-	-
30.2	1709.8	-	-	-	5.1	-	-	-	-
32.6	1707.4	70	10	20	-	-	-	-	-
34.0	1706.0	-	-	-	-	2.18	2.81	23.2	26.8
37.5	1702.5	75	25	-	-	2.22	3.03	26.7	4.7
45.5	1694.5	75	20	5	-	-	-	-	-
45.5	1694.5	-	-	-	41.4	-	-	-	-
47.6	1692.4	-	-	-	-	2.39	2.99	20.1	3.8
53.4	1686.6	75	10	15	-	-	-	-	-
54.4	1685.6	-	-	-	-	2.15	3.05	29.5	25.1
61.0	1679.0	35	65	-	-	2.33	2.74	15.0	1.5
61.0	1679.0	-	-	-	73.7	-	-	-	-
67.5	1672.5	75	10	15	-	-	-	-	-
68.0	1672.0	-	-	-	-	2.17	2.89	24.9	16.8
69.8	1670.2	55	45	-	-	-	-	-	-
75.6	1664.4	-	-	-	69.6	-	-	-	-
75.7	1664.3	44	55	1	-	-	-	-	-
75.8	1664.2	-	-	-	-	2.14	2.72	21.3	16.7
81.7	1658.3	-	-	-	-	2.12	2.82	24.8	30.6
81.8	1658.2	55	43	2	-	-	-	-	-
87.4	1652.6	60	40	-	-	-	-	-	-
87.5	1652.5	-	-	-	-	2.15	3.02	28.8	37.6
91.5	1648.5	-	-	-	-	2.24	2.68	16.7	4.2
91.5	1648.5	-	-	-	48.5	-	-	-	-
91.6	1648.4	60	35	5	-	-	-	-	-
94.8	1645.2	-	-	-	-	2.35	2.91	19.2	1.7
95.0	1645.0	25	75	-	-	-	-	-	-
95.0	1645.0	-	-	-	76.4	-	-	-	-
98.3	1641.7	-	-	-	-	2.13	2.87	25.8	33.3
98.5	1641.5	40	60	-	-	-	-	-	-
98.5	1641.5	-	-	-	66	-	-	-	-
101.5	1638.5	-	-	-	71.5	-	-	-	-
101.9	1638.1	-	-	-	-	2.12	2.65	22.0	80.7
103.0	1637.0	20	75	5	-	-	-	-	-
105.9	1634.1	-	-	-	-	2.18	2.65	18.3	15.5
106.0	1634.0	40	60	-	-	-	-	-	-
106.0	1634.0	-	-	-	56.5	-	-	-	-

* Haines (1966); vol% determined visually in thin-section; wt% insoluble residue after acid dissolution of carbonate
** Watkins and Walters (1966)
*** Kaibab is logged from 21 to 106 m for a total of 85 m, which is comparable to Shoemaker's measured thickness of 79-81 m.

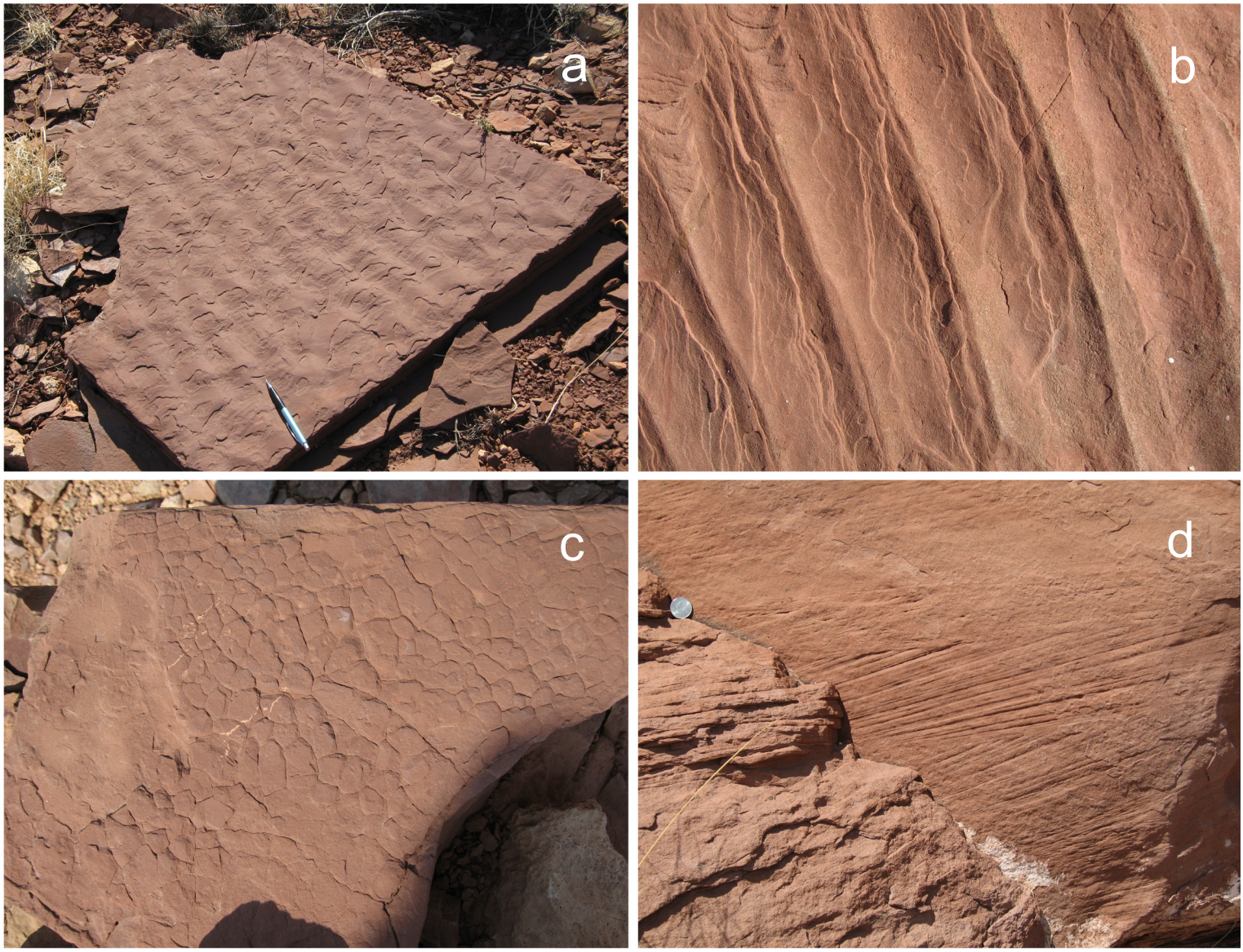

Fig. 2.4. Moenkopi sediments were deposited in a shallow-water coastal environment that was above wave base. A variety of wave-driven ripple marks, representing several types of current velocities, occur in the Moenkopi as illustrated in an oblique view of a slab (a) and an overhead view of another slab (b). Water often receded, producing dessication or mud cracks (c). Particularly important for the interpretation of the crater rim structure is the geopetal nature of cross-bedding exposed in the Moenkopi (d). This particular block is oriented normally, although the cross-beds in other blocks in the crater rim may be overturned.

Meteor Crater Quarry

Chirotherium minus
(amphibian)

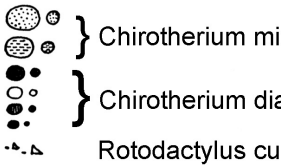

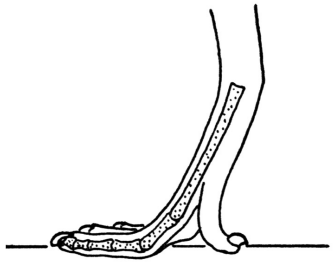

Rotodactylus cursorius
(reptile)

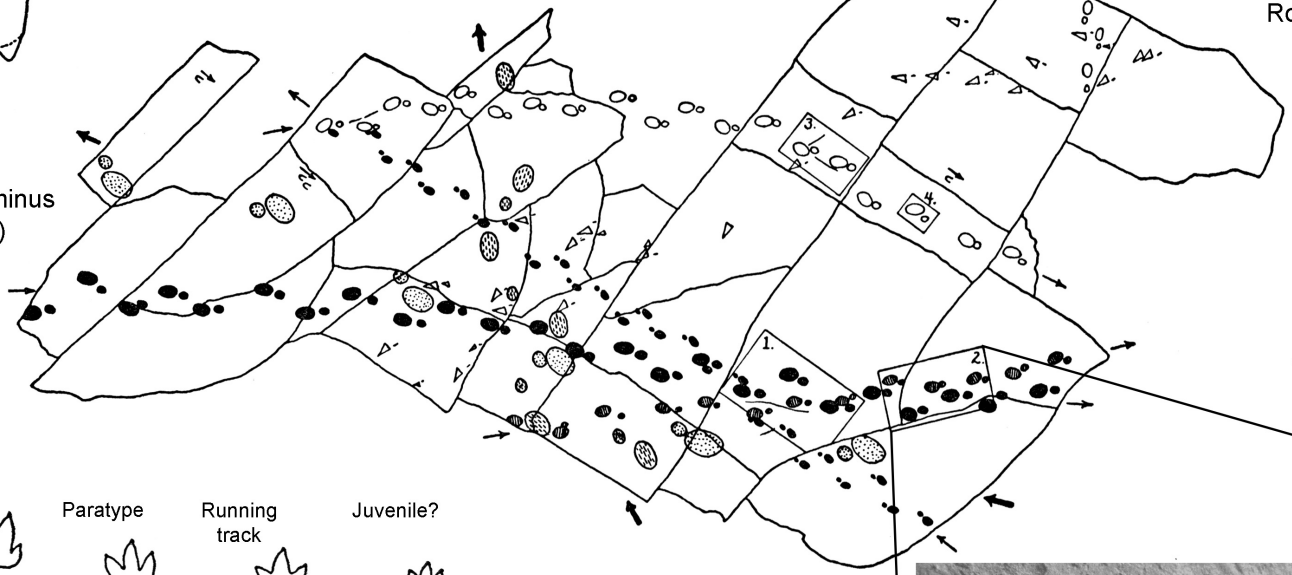

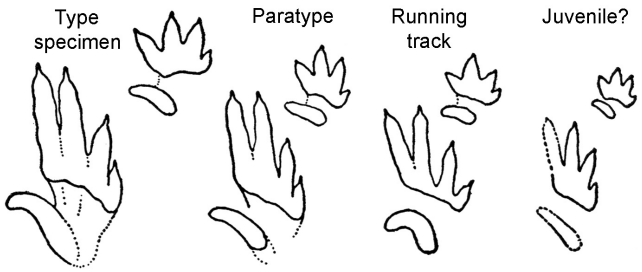

Chirotherium diabloensis
(amphibian)

Trackway Map

$\vec{c}$ = current indicators

50 cm

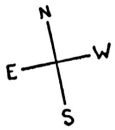

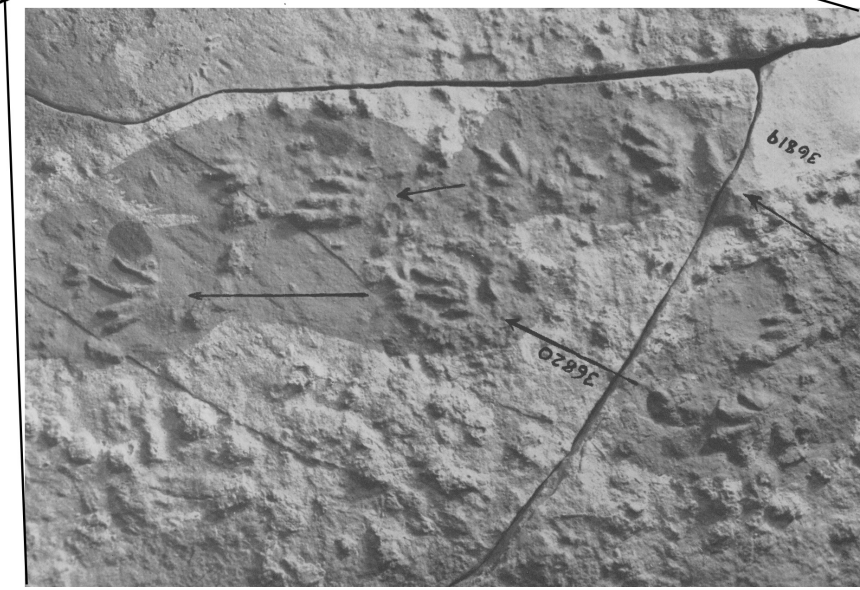

Fig. 2.5. Diagram of one of several trackways recovered from Meteor Crater Quarry. Montage was assembled from illustrations published by Peabody (1948).

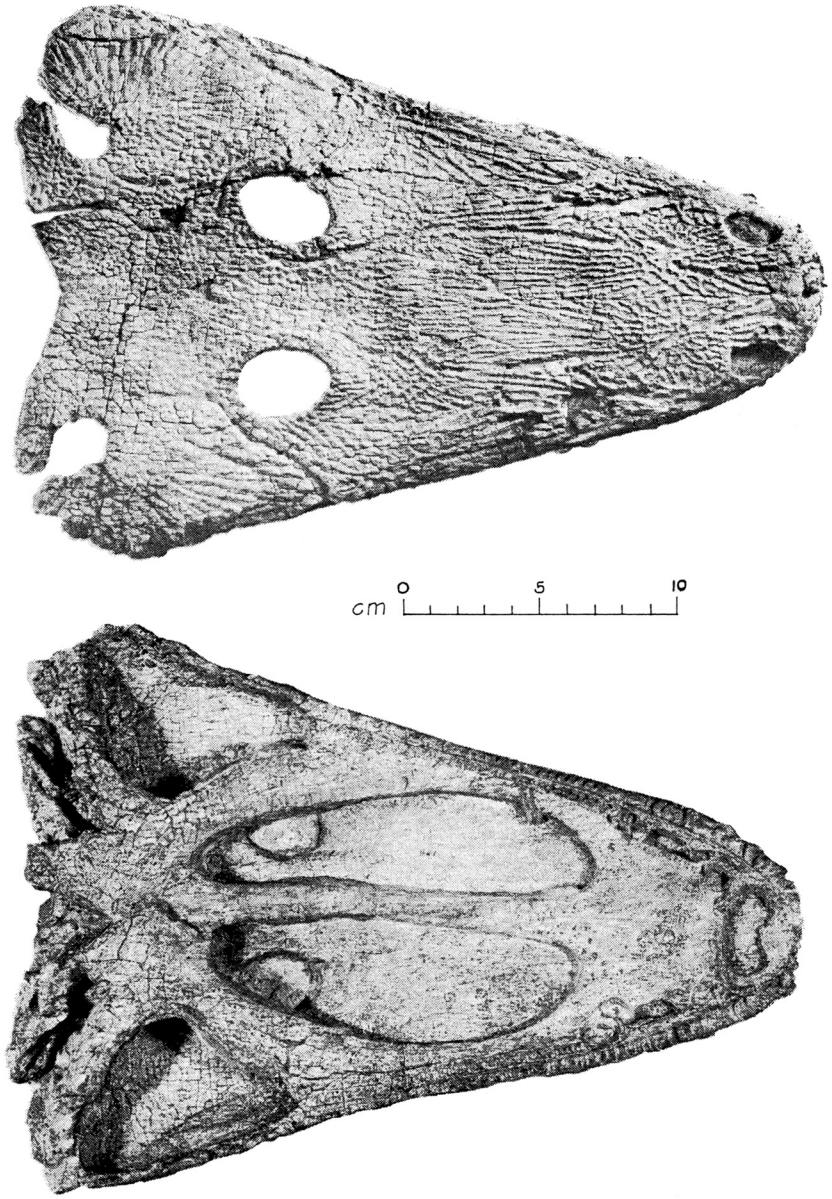

Fig. 2.6. A nearly complete skull of a new species of Labyrinthodont Family Capitosauridae that was recovered from the Moenkopi Formation in the Meteor Crater Quarry. This new species, *Parotosaurus peabodyi*, was described by Welles and Cosgriff (1965). The midline length of the skull is 28.3 cm (11.1 in). Teath are 6 mm long. There is room for 80 teeth in the peripheral row on each side of the maxillary, although Welles and Cosgriff suggest only half these were functional on the living animal. This is the type specimen for the species, but more than 20 skulls were recovered from the quarry, the largest of which had a midline length of 43.8 cm (17.2 in).

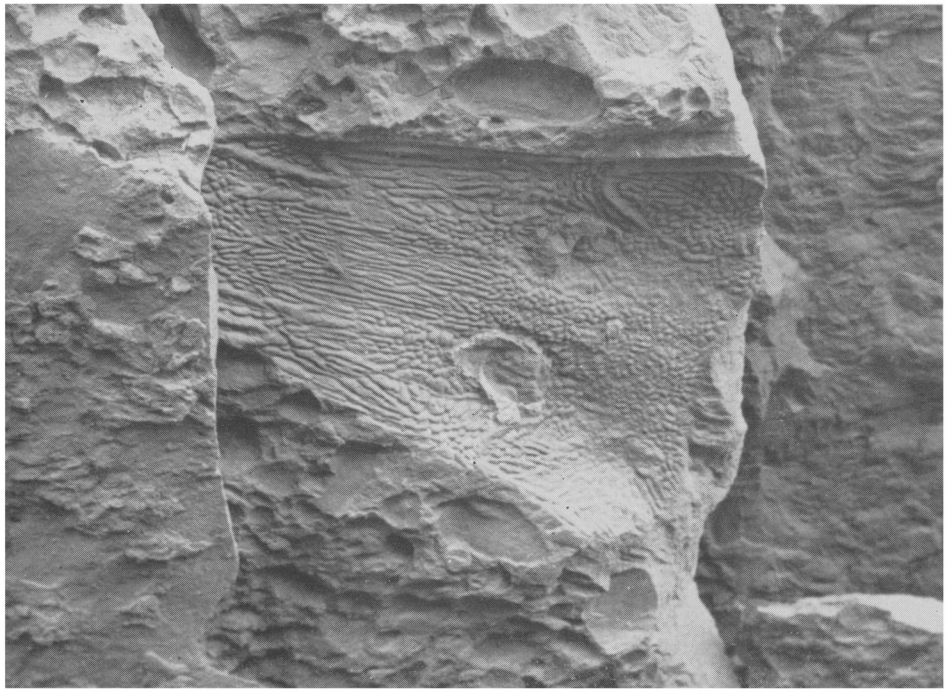

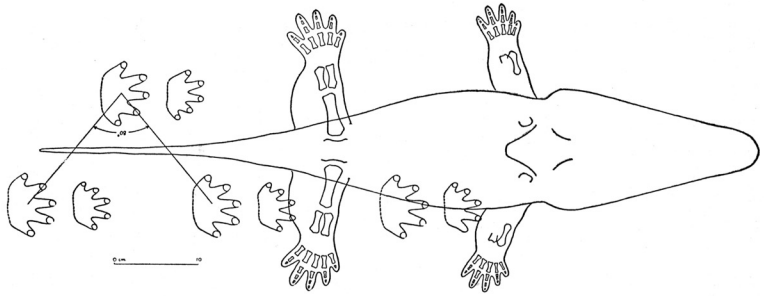

Impressions of capitosaurid skulls were also recovered a neaby quarry in Moqui Wash, including an example that occurs with shale pebbles in a fluvial foreset bed (top photograph from Peabody 1948). A sketch of a capitosaurid and the tracks it produced at Moqui Wash is also shown (bottom illustration, also from Peabody 1948).

Meteor Crater Quarry

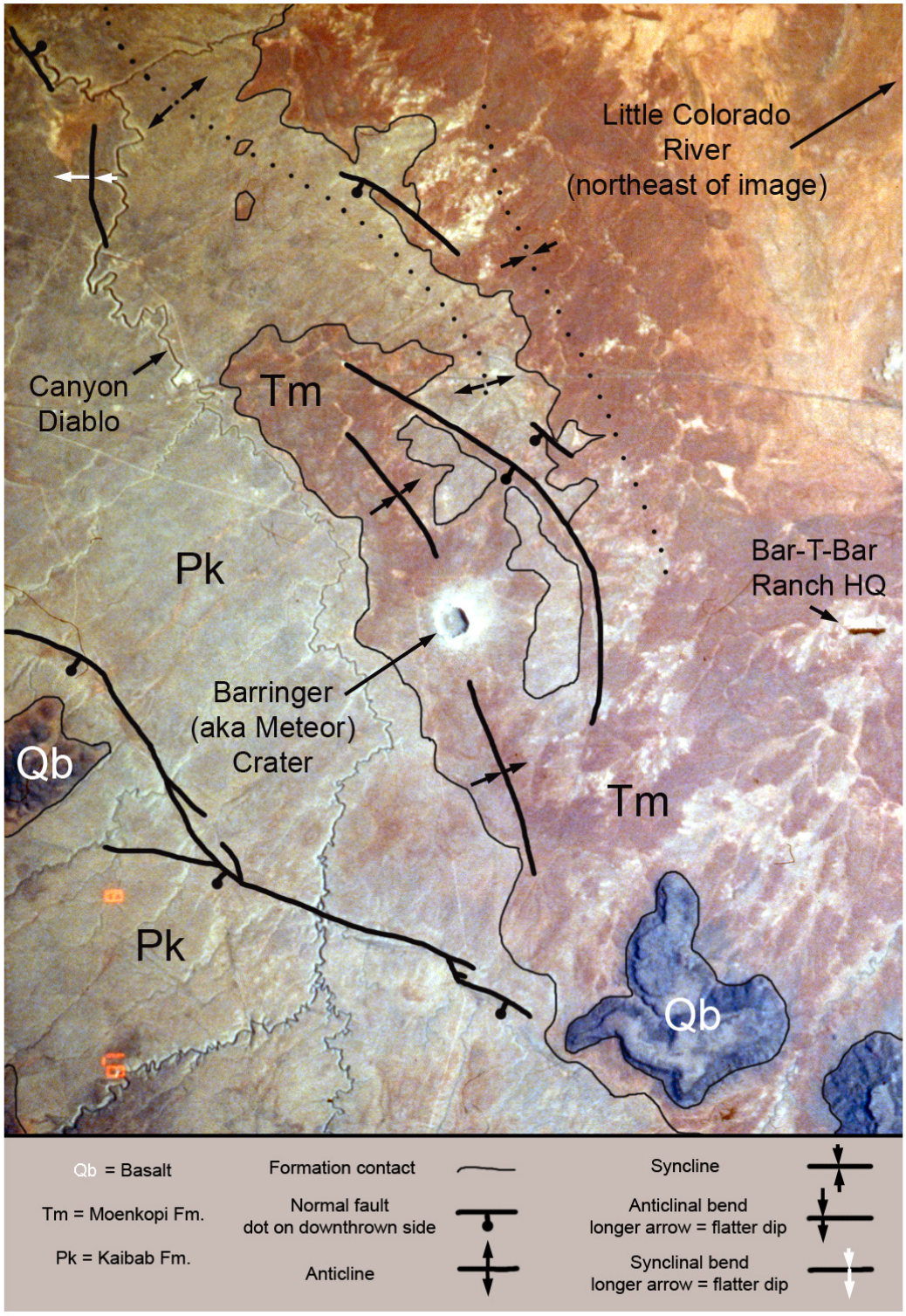

Fig. 2.7. Bedrock geologic map for the region around Barringer Meteorite Crater (*a k a* Meteor Crater) imprinted on an image taken from Space Shuttle Columbia (a cropped version of image #STS040-614-058). The formation contacts of Moenkopi (Tm) and Kaibab (Pk) are approximate, because Moenkopi is thin and becomes patchy in the vicinity of the crater. No effort was made to represent Pleistocene and Holocene alluvium or to distinguish Quaternary basalt (Qb) from talus derived from the basalt. Pleistocene impact ejecta and older subsurface lithologies exposed in the crater walls are also not mapped at this scale. Solid-line normal faults are mapped as seen in the image. Solid-line anticlines are inferred from geologic exposure and are consistent with the geologic map of Shoemaker (1958, as published in 1960). Anticlinal and synclinal bends are taken from Shoemaker (1960); solid lines represent more precise location of axes than do dotted lines.